International Journal of Fatigue 65 (2014) 71–77

Contents lists available at ScienceDirect

International Journal of Fatigue

journal homepage: www.elsevier.com/locate/ijfatigue

Cyclic behavior of a superferritic stainless steel at room and intermediate temperatures

S. Hereñú [a,*], M.G. Moscato [b], I. Alvarez-Armas [b], A.F. Armas [b]

[a] Instituto de Física Rosario, UTN-FRSN, Bv. 27 de Febrero 210 Bis, 2000 Rosario, Argentina
[b] Instituto de Física Rosario, UNR-FCEIA, Bv. 27 de Febrero 210 Bis, 2000 Rosario, Argentina

ARTICLE INFO

Article history:
Received 22 January 2013
Received in revised form 12 July 2013
Accepted 16 July 2013
Available online 7 August 2013

Keywords:
Superferritic stainless steels
LCF
Spinodal decomposition
DSA
Precipitates

ABSTRACT

This paper studies the fatigue behavior at room and intermediate temperatures of a superferritic stainless steel UNS S 44600 that had received different heat treatments. Thermal treatments at high temperature followed by water quenching produces needle-like Cr_2N precipitates that detrimentally affect the fatigue life of superferritic stainless steels. At intermediate temperatures, independent of previous thermal treatments, the occurrence of dynamic strain aging was manifested by a pronounced cyclic hardening rate, inverse dependence of the peak tensile stress with strain rate, a high dislocation density and modified dislocation arrangements. Cycling at intermediate temperature demodulates the spinodal decomposition with a fast velocity, improving the fatigue life of aged samples.

1. Introduction

Superferritic stainless steels contain high levels of Cr (22–3 wt.%), Ni and Mo (1–5 wt.%) and small quantities of interstitials elements (C and N <0.05 wt.%). In recent years, the worldwide demand has driven nickel and molybdenum prices to record high values. These steels, with low Ni content and reasonable Mo content, are a cost effective alternative that have attractive mechanical properties, high thermal conductivity and good corrosion resistance. Thus, these alloys are finding application in heat exchangers, the petrochemical industry and desalination and water recovery [1]. However, the ductility of these steels could be seriously weakened in intermediate temperature applications. Thus, the low cycle fatigue failure prevention is an important issue for structural components of these steels used at intermediate temperatures. In this sense, the phenomenon of dynamic strain aging (DSA) in ferritic stainless steels has been investigated in tensile and fatigue tests within the 300–600 °C range [2–4]. DSA occurs when solute atoms possess enough mobility to catch up with the moving dislocations and reduce dislocation motion during deformation. As DSA develops when the diffusivity of the solute atoms approaches the dislocation velocity, its occurrence depends on temperature and strain rate. During cyclic tests the usual manifestations of DSA are: an unusual increase in cyclic hardening rate, inverse dependence of the peak tensile stress with strain rate, plastic-deformation instability, enhanced dislocation density and modified dislocation arrangements [2–8]. On the other hand, in ferritic stainless steels aging between 400 °C and 500 °C leads to the well known "475 °C embrittlement" [9,11]. The "475 °C embrittlement" hardens and embrittles the steels at room temperature and it is believed to be caused by the spinodal decomposition (SD) of the ferrite phase into Cr-rich and Fe-rich phases [11].

Although for ferritic stainless steel all the possible embrittlement mechanisms are well-identified in literature, many doubts still remain on their consequences for cyclic deformation and fracture. The present paper aims to study the fatigue behavior of a superferritic stainless steel at room and intermediate temperatures after different thermal treatments. In doing so, at intermediate temperatures, the existence of a dynamic strain aging phenomenon (DSA) and the effect of fatigue on SD are evaluated.

2. Material and experimental procedure

The material used in this investigation is a UNS S 44600 superferritic stainless steel with the chemical composition given in Table 1. The steel was received in the form of hot-rolled cylindrical bars of 25.4 mm diameter. During the fabrication processes of the bars it is possible that an inhomogeneous dislocation structure and harmful phases such as chromium carbides or σ phase were formed [12]. Reheating ferritic stainless steels between 950 and 1100 °C and then cooling rapidly will dissolve the chromium carbides and σ phase and prevent re-precipitation during cooling [13,14]. However, these thermal treatments can also form

* Corresponding author. Tel.: +1 5403414808545.
E-mail address: herenu@ifir-conicet.gov.ar (S. Hereñú).

0142-1123/$ - see front matter © 2013 Elsevier Ltd. All rights reserved.
http://dx.doi.org/10.1016/j.ijfatigue.2013.07.012

Table 1
Chemical composition of UNS S 44600 (wt.%).

C	Cr	Mn	Cu	Si	V	Sn	N	S	Ni	P	Nb	Mo
0.022	23.44	0.75	0.08	0.29	0.12	0.008	0.062	0.002	0.3	0.019	0.1	0.08

Table 2
Thermal treatments applied to UNS S 44600.

TTW	1100 °C for 30 min followed by water quenching
TTA	1100 °C for 30 min followed by air cooling
TTW + AG	1100 °C for 30 min followed by water quenching and then heat treated 100 h at 475 °C
TTA + AG	1100 °C for 30 min followed by air cooling and then heat treated 100 h at 475 °C

chromium nitrides, if free nitrogen is present in the steel matrix. These precipitates detrimentally affect the mechanical properties and decrease fracture toughness at low temperature [15]. Therefore, two homogenization thermal treatments at 1100 °C for 30 min were carried out in the as-received bars, one ended with water quenching (TTW) and the other with air cooling (TTA). After the TTW the grain size was (77 ± 6) μm whereas after TTA was (81 ± 5) μm. An additional aging of 100 h at 475 °C were given to some TTW and TTA bars. This material is referred as aged (AG). Table 2 shows the different thermal treatments. Push–pull cylindrical specimens with a gauge length of 18.4 mm and a diameter of 5 mm were machined from the thermally treated bars.

Cyclic deformation tests were carried out with an Instron (model number 1362) electromechanical testing machine under plastic strain control using a fully reversed triangular form signal. The specimens were tested in air between 20 and 475 °C with a plastic strain range of 0.3% performed at a total strain rate of $2 \times 10^{-3}\ s^{-1}$. Between 20 and 500 °C, the strain rate dependence of the peak tensile stress was evaluated by changing the strain rate one order of magnitude during cyclic tests at a total strain range of $\Delta\varepsilon_t = 1.14\%$. The experimental procedure, already used in other materials [5–7], consisted of: at each temperature, starting at 20 °C, the sample was allowed to reach approximately 300 cycles with a strain rate of $2 \times 10^{-3}\ s^{-1}$. This number of cycles corresponds to an almost stabilized peak tensile stress (σ_1) in most of the tests performed at different temperatures. Then, without any interruption of the test, the strain rate was decreased to $2 \times 10^{-4}\ s^{-1}$ and after reaching stabilization, a peak tensile stress (σ_2) was measured. Stress increments were measured in the form $\Delta\sigma_{\text{strain rate}} = \sigma_2 - \sigma_1$. This procedure was repeated with increasing temperatures.

The microstructure and precipitates were examined using optical microscopy. Transmission electron microscopy (TEM) equipped with energy dispersive spectroscopy (EDS) was used to make a detailed study of the size and composition of the precipitates. Both replica and thin foil transmission electron microscopy techniques were used to identify the precipitates.

After fatigue tests, the fracture surfaces were analyzed using SEM. Dislocations structures were observed in a transmission electron microscope (TEM).

3. Results and discussion

3.1. Thermal treatments

The homogenization thermal treatments applied in this work are reported to be sufficient for preventing the formation of harmful $M_{23}C_6$ and sigma phase in ferritic stainless steels containing V and Nb [14]. Optical micrographs of the TTW samples show numerous small precipitates, with sizes of approximately 0.5 μm, distributed mainly inside the ferrite grains, Fig. 1a. New precipitates, too thin to be detected by optical microscopy, with a needle-like morphology are observed by TEM in the TTW samples, Fig. 1b. In Fig. 1c these needle-like precipitates are clearly visible in the dark field image (DF). This DF image was obtained using a lattice reflection of a hexagonal closed-packed structure, which is contained within the BCC ferrite phase, Fig. 1d. An EDS's analysis of extracted precipitates revealed the existence of two types of precipitates. In this sense, in TTW samples in addition to the expected NbC precipitates [14], Fig. 1e, other thin precipitates with high contents of Cr and N were detected, Fig. 1f. In ferritic stainless steel as well as in the ferrite phase of duplex stainless steel [15–17], particles identified as Cr_2N are formed after quenching from higher temperatures. Usually, precipitates of this kind occur at aging temperatures between 700 and 900 °C, but they have been found as a result of fast cooling from higher temperatures. Higher solution temperatures increase the solubility of nitrogen in ferrite and higher cooling rates improve the driving force for hexagonal closed-packed Cr_2N formation as a result of the supersaturation of nitrogen in the ferrite. According to Safsten [16], depending on the cooling rate different morphologies of Cr_2N can be observed. As the cooling rate increases, the precipitates' morphology changes from needle to cloud like. Hence, from the observed diffraction pattern, Fig. 1d, and the EDS measurements, Fig. 1f, it can be confirmed that after TTW needle-like Cr_2N precipitates are present in this superferritic stainless steel. Demo [18] reported that in AISI 446 ferritic stainless steel the precipitation of nitrides at grain boundary did not strongly affect the toughness, whereas, fine nitride precipitation on dislocations degrades the ductility of this steel. These precipitates reduce the dislocation mobility, decreasing the toughness of the materials. Nevertheless, no information about how Cr_2N precipitates affects fatigue has been reported for superferritic stainless steel. Attempting to avoid Cr_2N precipitation, TTA was employed. Fig. 2a shows the macroscopic structure of specimens with TTA. It turned out that the size of precipitates has increased significantly in comparison with TTW. Additionally, TEM images of TTA samples, Fig. 2b, give no evidence of needle-like precipitates. EDS's results of TTA samples show the presence of NbC as in TTW, but with a greater size (approx. 1.5 μm). Moreover, VC precipitates are also found, Fig. 2c.

In both TTW and TTA aged samples, a mottled contrast, typical of the presence of the spinodal decomposition, is clearly visible, Fig. 3.

3.2. Fatigue behavior

3.2.1. Cyclic response at 20 °C

Fig. 4 shows the cyclic response of the superferritic stainless steel UNS S 44600 at 20 °C after different thermal treatments. The TTW material attains a higher stress level than the TTA. On the other hand, as a consequence of aging, the highest stress levels were observed in the AG samples. The cyclic behavior of this steel, with TTA and TTW, is characterized by an initial cyclic hardening followed by cyclic softening, which ends in a saturation stage. In contrast, both the hardening and softening of AG samples are more pronounced and the saturation stage is never reached. Instead, an abrupt failure of the specimen is observed. The strong embrittlement of ferritic stainless steel in fatigue testing due to the SD is

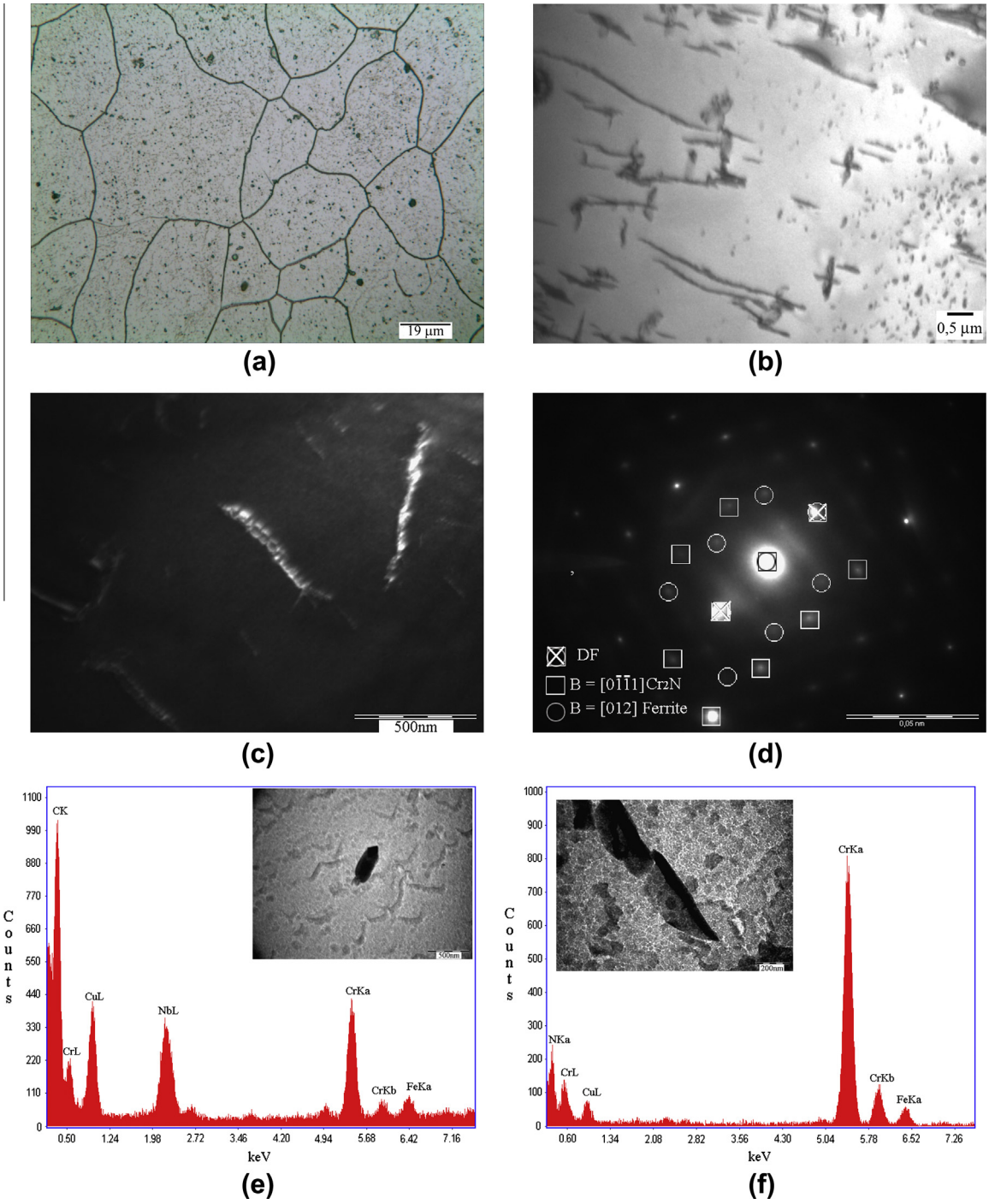

Fig. 1. Microstructures of UNS S 44600 with TTW: (a) optical image; (b) bright-field TEM image, (c) dark field TEM image, (d) superposed electron-diffraction pattern of nitrides and matrix (ferrite), (e and f) EDS analysis of precipitates.

well known [9,10]. But, the most surprising behavior is the pronounced embrittlement exhibited by the TTW steel. This can be attributed to needle-like Cr_2N precipitates [19]. SEM images taken from the fracture specimens at 20 °C are consistent with this assumption. While the TTW specimens' failure surfaces are essentially covered with brittle grains containing crystallographic rivers pattern, Fig. 5a, the fracture of the TTA specimen is characterized by ductile fatigue striations, Fig. 5b. The fracture surface of the AG steel shows a mixture of ductile and brittle areas, Fig. 5c. From the arguments presented so far, it can be reasoned that Cr_2N needles detrimentally affects the fatigue life of these superferritic stainless steels.

In order to analyze the correlation between the cyclic response and the dislocation structure, TEM observations were carried out. Fig. 6 shows the dislocation structure of samples fatigued to rupture at 20 °C. Interconnected dense loop patches around the Cr_2N needle-like precipitates separated by channels nearly free of dislocations characterize the dislocation arrangements seen in fatigued TTW specimens, Fig. 6a. In fatigued TTA specimens, Fig. 6b, dislocations walls and cells develop during cycling.

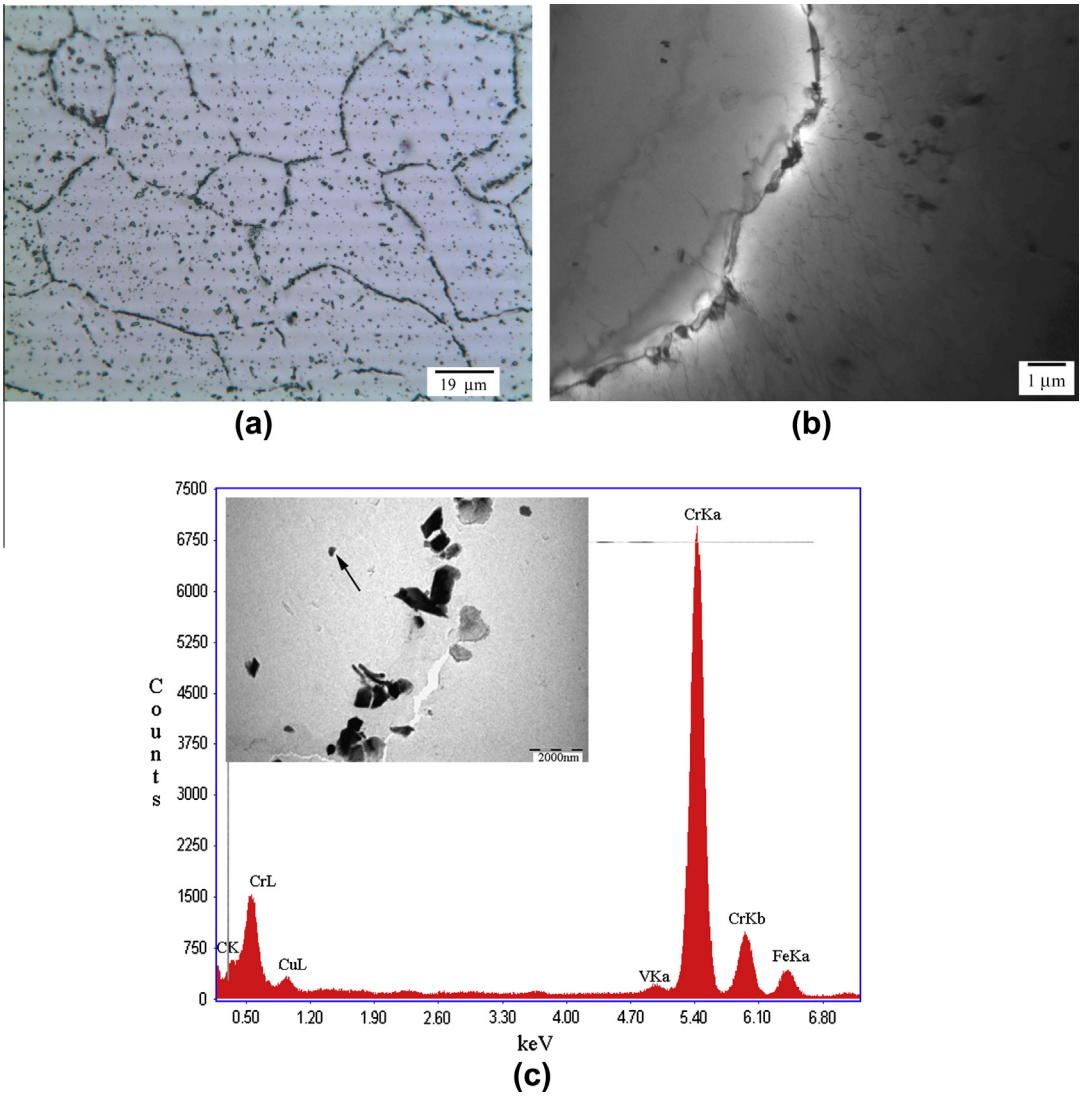

Fig. 2. Microstructures of UNS S 44600 with TTA: (a) optical image, (b) bright-field TEM image, (c) EDS analysis of VC precipitate.

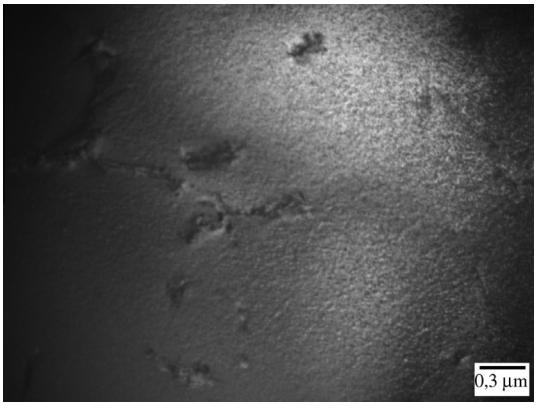

Fig. 3. Mottled contrast resulting from the spinodal decomposition of UNS S 44600 after 100 h at 475 °C.

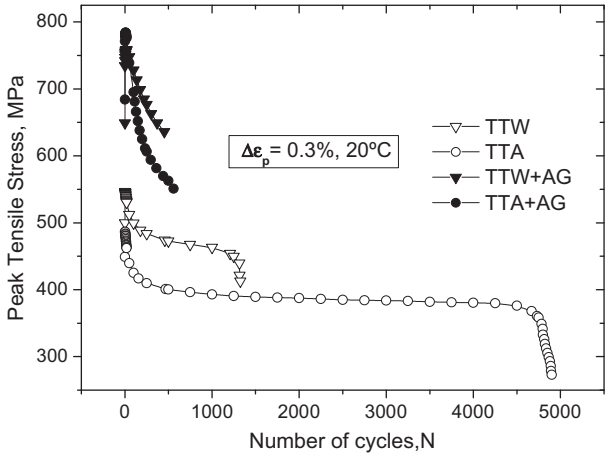

Fig. 4. Cyclic response of superferritic stainless steel UNS S 44600 at 20 °C.

Some microstructural differences can be pointed out for specimens tested in AG conditions. In TTW + AG specimens, the interconnected dense loop patches, previously observed in TTW cycled samples, are still found, but now the channels are full of dislocations, Fig. 6c. The difficulty of dislocation motion in the latter case creates a high dislocation density in order to accommodate plastic deformation, leading to brittle failure of the steel. Some aged ferritic grains also develop a dislocation arrangement, Fig. 6d, that resembles the dislocation bands and microbands

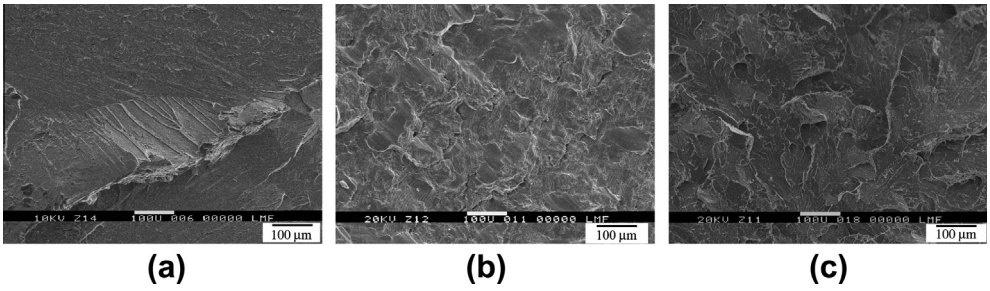

Fig. 5. SEM images of the fracture surface of UNS S 44600 samples cycled tested at 20 °C: (a) TTW, (b) TTA and (c) AG.

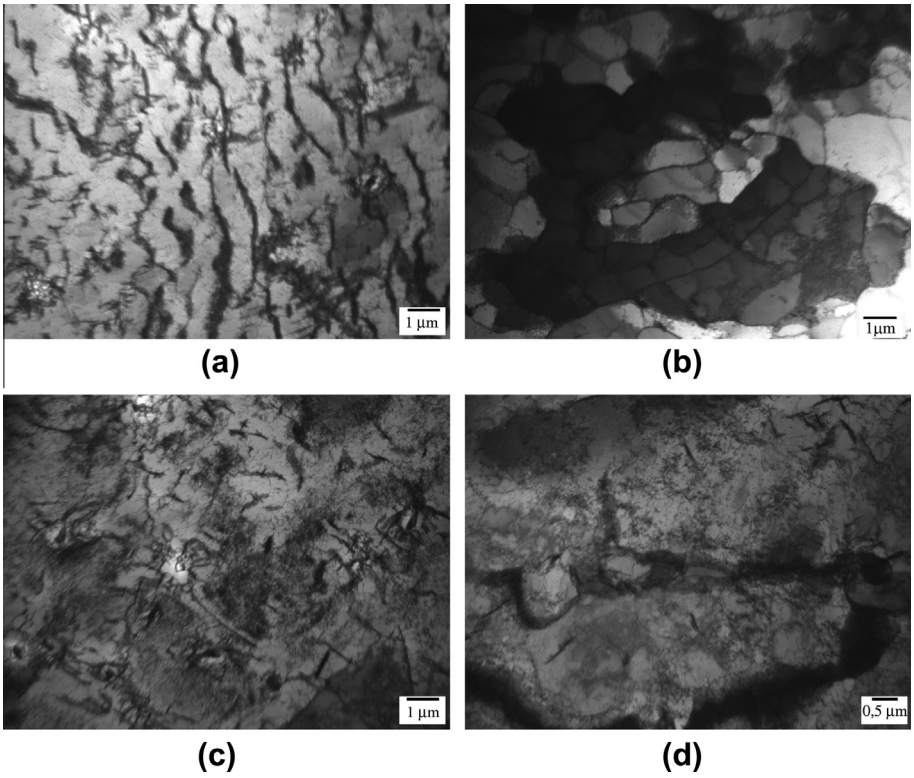

Fig. 6. Dislocation structure of UNS S 44600 cycled to failure at 20 °C: (a) TTW, (b) TTA, (d and c) TTW + AG.

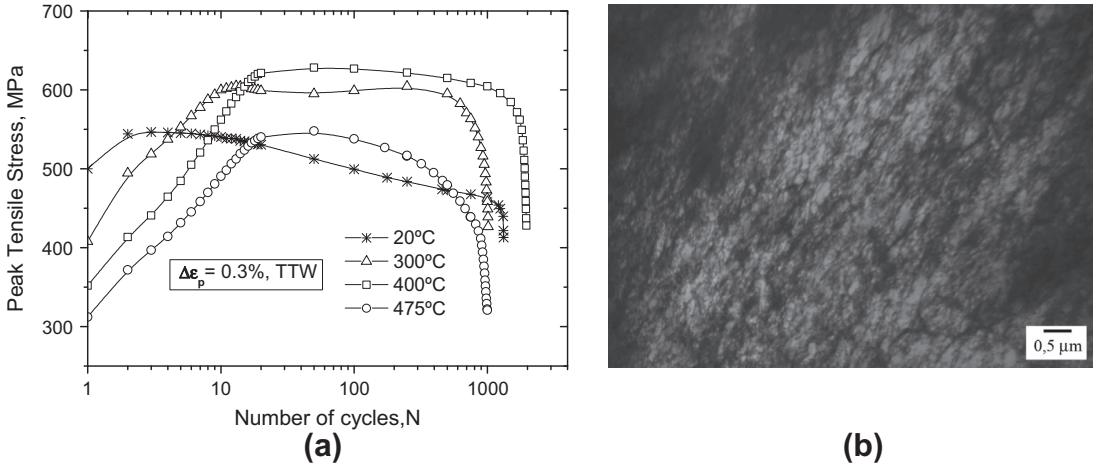

Fig. 7. Superferritic stainless steel UNS S 44600 with TTW: (a) cyclic response at different temperatures and (b) dislocation structure of a specimen cycled to failure at 400 °C.

observed in the ferrite phase of aged duplex stainless steel (DSS) fatigued at room temperature [20]. Hereñú et al. attributed the cyclic softening of aged DSS to the demodulation of spinodal decomposition within these structures. Therefore, the occurrence of the same kind of structure in this AG superferritic stainless steel could explain the observed cyclic softening, Fig. 4.

3.2.2. Cyclic response at intermediate temperatures

Fig. 7a shows the cyclic response of superferritic stainless steel UNS S 44600 with TTW at 20 °C and at intermediate temperatures. It is important to note that a pronounced initial cyclic hardening followed by a saturation stage is exhibited at intermediate temperatures. Such strong cyclic hardening has been established as a typical manifestation of DSA in ferritic stainless steels [2–4]. On the other hand, whereas at 300 °C and at 400 °C the saturation stage ends in rupture, at 475 °C a cycling softening stage sets in until fracture. TEM analysis shows a high dislocation density in samples tested between 300 °C and 475 °C, Fig. 7b. At these temperatures, uncondensed dislocation walls with poor defined channels are found, Fig. 7b. In contrast at 20 °C, interconnected dense loop patches separated by channels nearly free of dislocations are observed, Fig. 6a. A similar dislocation evolution with temperature has been reported in ferritic stainless steels [21] and in the ferrite phase of duplex stainless steel [2–4]. These researchers propose that at intermediate temperature the operation of a DSA mechanism creates a high rate of dislocation multiplication. Some aspects should be pointed out concerning the cyclic tests at 475 °C. Firstly, it should be noted that during cycling at this temperature both DSA and SD mechanisms can be active. However, samples aged at 475 °C for a time equivalent to this cyclic test give no evidence of SD through TEM observations. Secondly, at this temperature thermally activated dislocation motion gains importance enhancing the unpinning of dislocations from solute atoms. This fact can not only explain the short saturation stage but also the cyclic softening behavior observed at this temperature.

Though pronounced cyclic hardening and high dislocation density are often considered as evidences for the occurrence of DSA, inverse dependence of the peak tensile stress with strain rate is an even more sensible manifestation of DSA. Therefore, strain rate changes over one order of magnitude were carried out during cyclic tests at different temperatures in TTW and TTA samples, Fig. 8. At 20 °C and 500 °C, $\Delta\sigma_{\text{strain rate}}$ shows a normal behavior, exhibiting lower peak tensile stress for the slower strain rates. Between 200 and 400 °C an anomalous behavior, characterized by higher peak tensile stresses corresponding to slower strain rates, is observed. This DSA manifestation attains a maximum at 400 °C. Considering the embrittlement features of AG material, strain rate changes with these samples were performed only at 400 °C. It should be noted that SD does not prevent the occurrence of this DSA manifestation. To the authorś knowledge, DSA manifestation in aged ferritic steels has not yet been reported in literature.

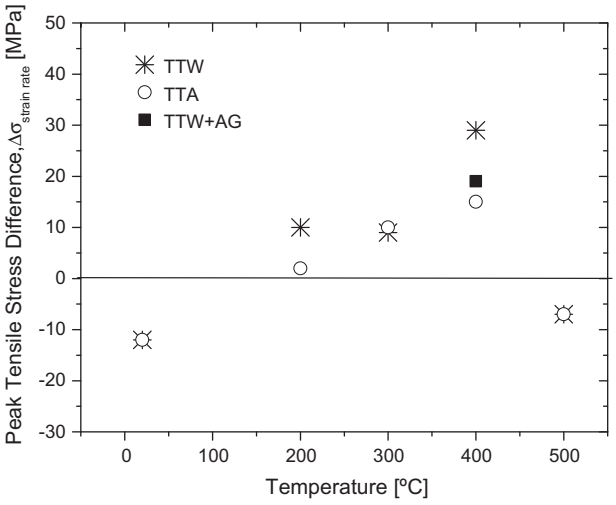

Fig. 8. Peak tensile stress difference vs. temperature of superferritic stainless steel UNS S 44600.

As the maximum effects of DSA are observed at 400 °C, this temperature was selected in order to evaluate the influence of previous thermal treatments on the cyclic response at intermediate temperature, Fig. 9a. In TTW and TTA specimens, a noticeable cyclic hardening rate during the first cycles is observed. Subsequently, a stabilization stage is attained. It is important to remark, that the cyclic hardening in TTW specimens is more pronounced than that exhibited by cycled specimens with TTA. In cyclic tests at 20 °C, the Cr_2N presence in TTW samples leads to higher stress levels but the cyclic hardening rate is the same as in TTA samples. Therefore, Cr_2N cannot be responsible for the pronounced cyclic hardening rate observed at 400 °C. On the other hand, in TTW samples a smaller size of NbC particles is found in comparison to TTA material. Therefore, TTW has a higher C content and a lower N content in the matrix than TTA. As the degree of DSA manifestations is greater in TTW samples than in TTA samples, it seems that C atoms accounts for the increase in DSA effects. In TTW + AG samples, a

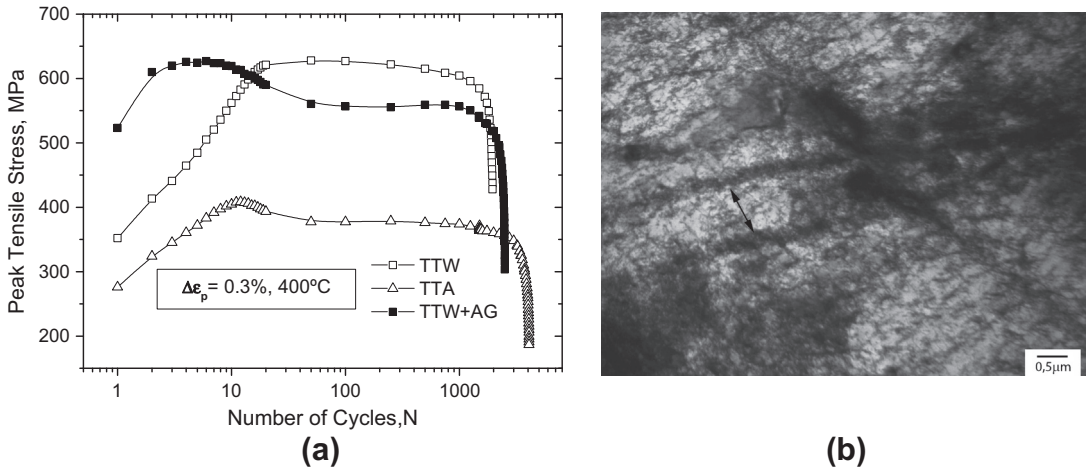

Fig. 9. Superferritic stainless steel of UNS S 44600 cycled at 400 °C: (a) with different previous thermal treatments and (b) dislocation structure of TTW + AG at rupture.

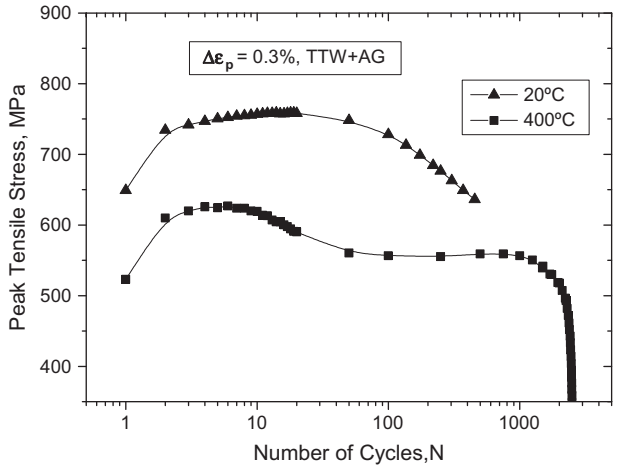

Fig. 10. Cyclic response of superferritic stainless steel of UNS S 44600 with TTW + AG.

slight initial hardening is followed by a softening stage that ends in a saturation stage. Fig. 9b shows dislocation bands developed during cycling at this temperature in TTW + AG samples, see arrow. In aged DSS, Hereñú et al [20] reported that the cyclic softening observed at intermediate temperature is attributed to the demodulation of SD inside localized dislocations bands. In the present steel, the same assumption could explain the cyclic softening observed in aged samples tested at 400 °C. Nevertheless, as DSA operates at this temperature, a high dislocation density between the dislocation bands is found. Thus, though the demodulation of SD produces softening, DSA produces hardening. Therefore, a saturation stage is finally achieved.

Finally, as regards AG samples, it should be noted that cycling at intermediate temperature is beneficial in improving the fatigue life over cycling at 20 °C, Fig. 10. It seems that the synergistic effect of temperature and cycling demodulates the spinodal decomposition more rapidly than that produced within the few dislocation bands seen at room temperature. This agrees with the observation of an early softening stage attained at intermediate temperature, associated with development of many dislocations bands where the demodulation of SD occurs, Fig. 9b.

4. Conclusions

The low cycle fatigue behavior of superferritic stainless steel UNS S 44600 at room and intermediate temperatures has been studied after conducting different thermal treatments. The main results are the following:

- Thermal treatments at high temperature followed by water cooling (TTW) produce needle-like Cr_2N precipitates that detrimentally affect the fatigue life of the superferritic stainless steels studied in this investigation.
- Regardless of the previous thermal treatments, cyclic testing at intermediate temperatures demonstrated the existence of dynamic strain aging (DSA) in superferritic stainless steel UNS S 44600. A pronounced cyclic hardening rate, inverse dependence of the peak tensile stress with strain rate, high dislocation density and modified dislocation arrangements are direct experimental indications of the occurrence of this phenomenon. The maximum DSA effect is observed at 400 °C. Moreover, TTW intensifies DSA due to the increase of C content in the matrix.
- The spinodal decomposition does not prevent the existence of DSA. Additionally, the synergistic effect of temperature and cycling demodulates the spinodal decomposition more rapidly than at room temperature improving the fatigue life of this steel.

Acknowledgements

This work was supported by the Agencia Nacional para la Promoción de la Ciencia y la Técnica (ANPCyT) and Consejo Nacional de Investigaciones Científicas y Técnicas (CONICET) of Argentine. The authors would like to thank Dr. Patricia Bozzano for helping in the characterization of the precipitates in this steel.

References

[1] Janikowski D, Henricks W. Super-ferritic stainless steels – the cost effective answer for heat transfer tubing REF: MP07-016. World Congress on Desalination and Water Reuse. Gran Canarias, Spain. October 21–26, 2007.
[2] Lee KO, Samson Yoon, Lee SB, Kim BS. Low cycle fatigue behaviour of 429EM ferritic stainless steel at elevated temperatures. Key Eng Mater 2004;261–263:1135–40.
[3] Avalos M, Alvarez-Armas I, Armas AF. Dynamic strain aging effects on low-cycle fatigue of AISI 430F. Mater Sci Eng A 2009;513–514:1–7.
[4] Tjong SC, Zhu SM. Creep and low-cycle fatigue behavior of ferritic Fe–24Cr–4Al alloy in the dynamic strain aging regime: effect of aluminum addition. Metall Mater Trans A 1997;28:1347–55.
[5] Armas AF, Avalos M, Alvarez-Armas I, Petersen C, Schmitt R. Dynamic strain ageing evidences during low cycle fatigue deformation in ferritic – martensitic stainless steel. J Nucl Mater 1998;258–263:1204–8.
[6] Hereñú S, Alvarez-Armas I, Armas AF. The influence of dynamic strain ageing on the low cycle fatigue of duplex stainless steel. Scripta Mater 2001;45:739–45.
[7] Gironés A, Llanes L, Anglada M, Mateo M. Cyclic deformation of superduplex stainless steels at intermediate temperatures. Metall Mater Trans A 2006;37:3519–30.
[8] Wu J-H, Lin C-K. Effect of strain rate on high- temperature low cycle fatigue of 17–4 PH stainless steel. Mater Sci Eng A 2005;390:291–8.
[9] Park KH, Lasalle JC, Schwartz LH. The low cycle fatigue behaviour of spinodally decomposed Fe- 26–1 Mo alloys. Acta Metall 1985;33:205–11.
[10] Akita M, Kakiuchi T, Uematsu Y. Microstructural changes of high-chromium ferritic stainless steel subjected to cyclic loading in 475 °C embrittlement region. Proced Eng 2011;10:100–5.
[11] Soriano-Vargas O, Avila-Davila EO, Lopez-Hirata VM, Cayetano-Castro N, Gonzalez Velazquez JL. Effect of spinodal decomposition on the mechanical behavior of Fe–Cr alloy. Mater Sci Eng A 2010;527:2910–4.
[12] Guimaraes AA, Mei PR. Precipitation of carbides and sigma phase in AISI type 446 stainless steel under working conditions. J Mater Process Technol 2004;155–156:1681–9.
[13] Nooning RG. Jr. Effect of stabilizing elements on the precipitation behavior and phase stability of type 409 ferritic stainless steel. Master of Science in Materials Science and Engineeering. University of Pittsburg; 1999.
[14] Kuzucu V, Aksoy M, Korkut MH. The effect of strong carbide-forming elements such as Mo, Ti, V and Nb on the microstructure of ferritic stainless steel. J Mater Process Technol 1998;82:165–71.
[15] Van Zwieten ACTM. Some considerations on the toughness properties of ferritic stainless steels: a brief review. Int J Pres Ves Piping 1993;56:1–31.
[16] Safsten A. Quantitative phase analysis of duplex stainless steel as a function of heat treatment M.Sc. Thesis in engineering physics, Lulea University of Technology; 2009.
[17] Liu P. Investigation of precipitation of β-Cr_2N in duplex stainless steel SAF 3207 HD, Sandvick Technical Report 080631TE. Sandvick Mater Technol 2008.
[18] Demo J. Mechanism of high temperature embrittlement and loss of corrosion resistance of AISI 446 stainless steel. Corrosion NACE 1971;27(12):531–44.
[19] Hereñú S, Moscato MG, Alvarez-Armas I, Armas AF. Cyclic behavior of a superferritic stainless steel at room and intermediate temperatures. In: XVI international colloquium mechanical fatigue of metals, Czech Republic; 2012.
[20] Hereñú S, Sennour M, Balbi M, Alvarez-Armas I, Thorel A, Armas AF. Influence of dislocation glide on the spinodal decomposition of fatigued duplex stainless steels. Mater Sci Eng A 2011;528:7636–40.
[21] Mughrabi H, Christ H-J. Cyclic steels deformation and fatigue of selected ferritic and austenitic steels specific aspects. ISIJ Int 1997;37(12):1154–69.